JOINT EUROPEAN TORUS JET

JET–P(87)62

S.K. Erents, J.A. Tagle, G.M. McCracken, P.C. Stangeby
and L de Kock

The Dependence of Tokamak Edge Conditions on Global Plasma Parameters in JET

The Dependence of Tokamak Edge Conditions on Global Plasma Parameters in JET

S.K. Erents[1], J.A. Tagle[2], G.M. McCracken[1], P.C. Stangeby[3], and L de Kock[1]

JET-Joint Undertaking, Culham Science Centre, OX14 3DB, Abingdon, UK

[1]UKAEA Culham Laboratory, Abingdon, Oxen OX14 3DB, UK (UKAEA/Euratom Fusion Association)
[2]JET-Joint Undertaking, Culham Science Centre, OX14 3DB, Abingdon, UK
[3]Institute for Aerospace Studies, University of Toronto, Canada M3H 5T6

Preprint of Paper to be submitted for publication in
Nuclear Fusion

ABSTRACT.

Measurements have been made of the plasma parameters in the boundary layer over a wide range of operating conditions in JET. The plasma currents have been varied from 1MA to 5MA and the average density in the range from 1 to 5×10^{19} m^{-3}. It has been observed that the edge density increases with line average density and the edge temperature decreases. Emphasis has been placed on testing data under steady state conditions of plasma current and density.

The temperature and density at the last closed flux surface (LCFS)has been modelled using global particle and energy balance. It is shown that good quantitative agreement is obtained with experimental data for the density and the total particle and flux. In a second stage using the global energy balance a crude attempt is made to estimate the impurity influx and hence the radiation from the plasma. Results give the right order of magnitude and the correct trends for the variation of the edge temperature with density and input power.

1. INTRODUCTION

In an earlier paper the tokamak edge conditions in JET ohmic plasmas were described for a modest range of global plasma parameters[1]. Some applications of the edge data to calculations of sputtering yields and impurity atom screening in the scrape off layer (SOL) were discussed. Recent measurements of edge parameters for other large tokamaks have been described in references (2 and 3) and a summary of earlier data on smaller machines is given in reference (4).

One of the principle objectives of edge diagnostics is to try to extrapolate to parameters typical of ignition conditions and to see whether there are ways of keeping the impurity influx under control as the heating power and the power generated by α particle production is increased. In the present paper we describe experimental measurements of the edge temperature, density and particle flux over a wide range of operating conditions in ohmic discharges, for plasma currents from 1 MA to 5 MA and for plasma average densities from 1 to 5 x 10^{19} m^{-3}. A clear pattern of behaviour is observed with edge temperatures increasing as the input power is increased and decreasing as the average density is increased. These experimental data are explained quantitatively in terms of the overall power and particle balance. Scaling relationships for the edge temperature and density are also derived.

2. EXPERIMENT

Measurements are made in two positions in the torus, fig. 1. At the top of the vessel in octant 5 an array of six probes is driven in vertically and can be moved between discharges. There are three probes on each side of the probe drive facing both the ion drift and the electron drift directions. Over a series of similar discharges a detailed profile can be built up for the region between the last closed flux surface (LCFS)

and the wall. In the carbon tiles surrounding the ICRH antenna in Octant 2 there are two probes built into the structure[5]. These probes are at a distance of 15 and 27 mm from the edge of the plasma (allowing for field ripple). The potentials of all probes are typically swept from - 100 to + 10 V over a period of 50 ms, 38 times during a single discharge. From the voltage-current characteristic the ion saturation current I_s, the electron temperature T_e, and the floating voltage V_f are calculated using a non-linear least square fit. More details of the probes and their operation have been presented in previous papers[1,5,6].

The results from the top probes and the antenna probes have been compared. To do this it is necessary to correct first for the fact that the top probe drive is at an angle of about 20° to the magnetic surfaces and secondly because the magnetic surfaces are compressed at the mid plane by a factor of approximately 2 compared with the top probe position. When these factors are taken into account the plasma parameters at the limiter edge (ie the LCFS) and the e-folding length of the profiles can be compared. For the limited data available good agreement is generally obtained, but the data from the antenna probes, where only two points on the profile are obtained, result in larger errors for the value of the parameters at the LCFS. The top probe collects data on the profiles not only by measuring at 3 radial positions but also by virtue of spontaneous slow movements of the plasma boundary during a discharge.

3. RESULTS

3.1 Ion flux, electron temperature and density

Typical radial profiles for the ion saturation current density ($I_s(r)$) and electron temperature ($T_e(r)$) are shown in figure 2. These results were obtained using the top probe array and are similar to those previously

reported (1). Exponential decays in $I_s(r)$ over 2 orders of magnitude, and $T_e(r)$ over 1 order of magnitude from 10-200 mm behind the LCFS have been recorded. From these data the edge density, $n_e(r)$, can be calculated assuming $T_e = T_i$. A comparison with data taken at the mid-plane, using the two probes on the antenna tiles, is also shown in figure 2. Here the field line compression between torus top and mid-plane is taken into account by calculations from the magnetic data. The mid-plane data are referred to the top of the torus.

Most of the data reported in this paper are from the fixed probes in the RF antenna tiles. Here exponential decays are assumed, and the data are extrapolated 15 mm to the LCFS. This avoids quoting results at an arbitrary radius inside the SOL, but assumes that the e-folding length does not vary across the leading edge of the RF antenna. There is some evidence for this assumption from the top probe data, which have shown no discontinuity in profiles right up to the LCFS.

The effect of mean plasma density $\bar{n}_e$ on edge parameters is shown for a single ohmic discharge with a density ramp during the plasma current flat-top, (figure 3). Under these non-steady-state conditions it is usual to find the ion saturation current density (I_s) to be fairly independent of $\bar{n}_e$, but the edge temperature T_e always falls markedly with increasing $\bar{n}_e$. Since the edge density n_e locally is related to the flux and temperature by the expression

$$n_e = 2I_s/e\,C_s \qquad (1)$$

where the ion sound speed $\quad C_s = \{k(T_e + T_i)/m_i\}^{\frac{1}{2}}$

it is expected that $n_e(a)$ will rise with $\bar{n}_e$ as illustrated. In non-steady-

state the exact dependence of $n_e(a)$ and $T_e(a)$ on $\bar{n}_e$ varies from shot to shot, but is usually in the range $n_e(a) \propto \bar{n}_e^{1 \text{ to } 2}$ and $T_e(e) \propto \bar{n}_e^{-2 \text{ to } -3}$.

To avoid these variations we have found it important to select data during ohmic discharges in which $\bar{n}_e$ is not changing rapidly. This is usually towards the end of the plasma current flat-top for discharges without a density ramp. We believe that the plasma conditions from which the rest of the data reported here are taken are close to steady state in terms of power balance and particle balance. Probable exceptions, however, are the 5 MA discharges in which only short plasma current flat-tops can be obtained, and in which significant power is frequently deposited on the torus inner wall.

The dependence of ion saturation current (or ion flux density $\Gamma_\parallel$) and electron temperature ($T_e(a)$) on $\bar{n}_e$ is shown in figures 4 and 5 for a range of plasma currents from 1 to 5 MA[7]. Data have been taken from an extensive data bank collected over several months and all are ohmic discharges in deuterium defined by a set of 8 discrete limiters at the outside mid plane. Data with unusually low loop volts have been rejected; if the loop volts are low, (indicating higher central temperatures for a given plasma current) then the edge temperatures are higher than depicted in figure 5.

The particle flux density increases with plasma current but is almost independent of $\bar{n}_e$, for fixed I_p, within the scatter between different shots, (figure 4). For the purpose of the model to follow it is useful to consider the scaling of the plasma current, I_p, in terms of ohmic power, P_Ω. We find from JET experimental data that $P_\Omega \approx 0.7\ I_p^{1.15}$. The data set shown in figure 4 can be represented by the empirical relationship:

$$\Gamma_{\parallel} = 2 \times 10^{3} I_p^2 = 2.7 \times 10^{3} P_{\Omega}^{1.75} \qquad (2)$$

where P_{Ω} is the ohmic power in MW, $\Gamma_{\parallel}$ is in A m^{-2} and I_p is in MA. Eqn.(2) implies no dependance of $\Gamma_{\parallel}$ on $\bar{n}_e$. However, operationally it is difficult to vary $\bar{n}_e$ by more than a factor of 2 at constant I_p. The fact that $\Gamma_{\parallel}$ does not change significantly at constant current may be due to the edge temperature decreasing with increasing density, as discussed later.

A similar empirical relationship can be found to represent the temperature data set, figure 5.

$$T_e = 6 \times 10^{39} \bar{n}_e^{-2} P_{\Omega}^{1.9} \ [eV] \qquad (3)$$

for n_e in units m^{-3} and P_{Ω} in MW.

From the radial profiles of the parallel flux we can calculate the total flux of particles reaching the limiter Γ_L. This is expressed as

$$\Gamma_L = \int_a^{r_w} \frac{H \ \Gamma_{\parallel}(r) \ dr}{e} \qquad (4)$$

where H is the total wetted height of the limiter, a is the radius of the last closed flux surface and r_w is the radius of the wall. We have to assume poloidal asymmetry in order to do the total integration. The results are shown in fig.6.

Using equation 1, and assuming $T_e = T_i$, we can derive local values of n_e from the measured I_s and T_e. The results are shown in fig.7. It is observed that the data at different currents now overlap and that overall the data approximately fits a square law. This is discussed in more detail in section 4.2.

Considering the empirical relationships (2) and (3) together with equation (1) it follows that the edge density $n_e(a)$ should be proportional to $\bar{n}_e$. An approximate empirical expression for $n_e(a)$ is

$$n_e(a) \approx 0.055\ \bar{n}_e \cdot P_\Omega^{0.8} \cdot m^{-3} \qquad (5)$$

However a least squares fit to the data in figure 7 shows that $n_e(a)$ rises less steeply than linear with $\bar{n}_e$ at low I_p, and more steeply than linear at high I_p. If we take $n_e(a)$ data at different plasma currents but with constant $T_e(a)$ then we find that $n_e(a)$ is to a good approximation proportional to $\bar{n}_e^{\,2}$, fig. 7.

3.2 Power Balance

The power flux to the limiters P_L may be calculated from the measured density and temperature profiles. The total power is the integral of the power density over the radial profile

$$P_L = \int_a^{r_w} \gamma_s . H .\ \Gamma_\parallel(r)\ T_e(r)\ dr$$

$$= \int_a^{r_w} \gamma_s . H .\ \Gamma_\parallel(a)\ \exp\left(\frac{-r}{\lambda_\Gamma}\right) T_e(a)\ \exp\left(\frac{-r}{\lambda_{T_e}}\right) dr. \qquad (6)$$

where γ_s is the sheath energy transmission factor, H is the total wetted height of the limiters, and λ_Γ, λ_T are the scrape-off lengths for particle flux and temperature. The change in secondary electron yield with electron energy, which is required to calculate the sheath transmission factor, has been measured experimentally for carbon samples exposed to the JET

plasma[8,9]. These data have been used to calculate the sheath transmission factor as a function of electron temperature and hence to calculate P_L. It is assumed that $T_e = T_i$, although there are no experimental measurements of T_i and collisions are of marginal frequency to ensure equipartition.

Assuming that the distance between the LCFS and wall is large compared with λ_Γ or λ_{T_e} (which is normally true in JET), then equation 6 may be integrated to obtain

$$P_L = \gamma_s H \, \Gamma_\parallel(a) . \, T_e(a) . \lambda_p \, \ldots\ldots \, (W) \qquad (7)$$

where the power scrape-off length $\lambda_p = \lambda_\Gamma \lambda_{T_e} / (\lambda_\Gamma + \lambda_{T_e})$. λ_p can be measured directly with thermocouples or an infra-red camera. Limited data from the I.R. camera show reasonable agreement with scrape-off lengths measured by the Langmuir probe[10].

Taking values of P_L as calculated from equation (7) we can check the validity of the global energy balance, ie:

$$P_L = P_\Omega - P_R = \gamma_s . H . \lambda_P . \Gamma_\parallel(a) \; T_e(a) . \qquad (8)$$

where P_R is the radiated power, measured by bolometers at the wall[11]. The total wetted height of the limiters is only a weak function of P_Ω in JET. In carrying out the integration we have had to assume a poloidal and toroidal symmetry of the edge parameters due to the limited experimental data. We have also included the power deposited on the RF antennae which is ~ 30% of the total power conducted to the edge. The measured values of P_L have been plotted against $(P_\Omega - P_R)$ in figure 8. There is clearly a linear relationship, basically validating equation (8). The absolute value

of P_L is a factor 2 - 2.5 lower than the power balance predicts. This could be due to toroidal and poloidal asymmetries resulting in different powers and different wetted areas to each limiter. The uncertainty in the position of the LCFS at the top of the torus (~ 20 mm), due to the finite mesh size of codes used to calculate magnetic surfaces, makes it difficult to quantify asymmetries by comparing antenna and top probe data. The estimated uncertainty in the position of the LCFS is approximately 2-3 mm at the mid-plane where it is well defined by the limiters. Another possible omission is the charge exchange power (P_{cx}), although in most machines this is found to be small compared with P_Ω[12]. It is possible that non-thermal plasma components cause γ_s to be underestimated. It is also possible that heat-loading in the first ~ 1 cm from the LCFS, at the mid-plane, is not correctly inferred from measurements made further out radially.

3.3 Radial diffusion in the edge

The cross-field diffusion coefficient $D_\perp$, in the edge can be estimated from measurements of λ_n plus a theoretical relation such as

$$D_\perp \simeq \lambda_n^2 C_s/L_c \qquad (9)$$

where L_c is the connection length between limiters. For a toroidal belt limiter $L_c = \pi R q_s$, q_s being the safety factor. For a non-circular plasma such as JET and a discrete, as distinct from a continuous toroidal limiter, eq(10) under-estimates $D_\perp$ by a factor, 4 typically. A more sophisticated analysis has been developed which takes into account plasma non-circularity and the discrete nature of the limiters[13]. The analysis has been used to calculate the values of $D_\perp$ shown in fig.9. $D_\perp$ is observed

to fall with density approximately as $\bar{n}_e^{-1}$.

Two pieces of evidence indicate that $D_\perp$ varies approximately as the square root of the local temperature:

(a) For any individual discharge the density profile in the SOL, $n_e(r)$, closely approximates to an exponential decay over a few orders of magnitude, i.e. the characteristic scale length λ_n is a constant over this region. Since temperature also varies radially, $T(r)$, then the sound speed does as well, $c_s(r) \propto T(r)^{1/2}$, implying from eqn.(9) that $D_\perp$ varies radially in the SOL as $T^{1/2}$. The values of $D_\perp$ plotted in Fig.9 were calculated using $T_e(a)$ and are therefore the values at the LCFS, $D_\perp(a)$.

(b) Turning to the collection of results of $T_e(a)$ for different values of $\bar{n}_e$, fig.5, the observations that $T_e(a) \propto \bar{n}_e^{-2}$, and $D_\perp(a) \propto \bar{n}_e^{-1}$, approximately, gives $D_\perp(a) \propto T_e(a)^{1/2}$.

4. DISCUSSION

4.1 The role of global plasma parameters on edge conditions

We first discuss the relationship between the edge plasma properties, principally $n_e(a)$ and $T_e(a)$ and the primary properties of the discharge, such as $\bar{n}_e$ and I_p. Clearly, it would be of considerable value to determine the mechanisms governing the dependence of edge conditions on global parameters so that predictions for future operating conditions could be made.

The modelling is carried out at two levels of simplification. In the basic model, section 4.2, an attempt is made to explain the gross features of the plasma edge by calculating $n_e(a)$ and $T_e(a)$ in terms of P_Ω, P_R and $\bar{n}_e$

as input data, employing simple particle diffusion and energy conservation models. In the subsequent section 4.3, an attempt is made to transfer the quantity P_R from the input to the calculated category by accounting in a simplified way, for sputtering and radiation in a self-consistant manner. We have seen experimentally that the edge temperature decreases as density increases. It is well known that the sputter yield decreases with ion energy thus it is to be expected that the impurity influx will also decrease as the density rises. The tendancy for the plasma to self-regulate its edge temperature by a feed-back mechanism has previously been pointed out[14, 15] and is reproduced here in a convenient analytic formulation.

4.2 A basic model

In the basic, or zeroth order modelling, one seeks to explain the principal measured edge quantities - namely the total deuteron outflow to the limiters, Γ_L, the edge density $n_e(a)$, and the edge temperature $T_e(a)$ - in terms of the global machine parameters - namely the total power input P_H ($P_H = P_\Omega$ for ohmic heating), P_R and $\bar{n}_e$. We consider first the edge density, $n_e(a)$, fig. 6. A simple diffusion model, deriving originally from Engelhardt et al[16], can be shown to give the relation[17]

$$n_e(a) \approx \frac{\overline{\sigma v}_{iz}}{6\,\bar{v}_n}\,\lambda_T\,\bar{n}_e^{\,2} \qquad (10)$$

between the edge density and the average plasma density, where $\bar{v}_n$ is the average inward velocity of the neutral hydrogen re-cycling from the limiter and $\overline{\sigma v}_{iz}$ is the average electron impact ionisation rate over the mean free path of the neutral hydrogen. The factor 6 is related to the $n_e(r)$ profile

and reflects a small assumed peaking factor, $\bar{n}_e \approx 1.7\ n_e\ (r/a = 0.9)$. The relationship[17] is very similar to that derived independently by Alexander et al[2].

A full test of this model requires that the value of $\bar{v}_n$ be known. Since this quantity is the result of a number of contributions, including direct molecular ionisation, Franck Condon atom ionisation, ion backscatter, charge exchange, etc, it can only be established by neutral codes such as the DEGAS Monte Carlo code[18]. In the absence of direct information for JET conditions, a value of $\bar{v}_n = 3 \times 10^4$ m/s (10 eV D) is estimated. To a good approximation $\overline{\sigma v}_{iz} \approx 3\times10^{-14}$ m^3/s, i.e. the maximum value, since the neutrals tend to penetrate until reaching a plasma zone where electrons have this rate. The scrape-off layer thickness for particle flux, λ_Γ is independent of $\bar{n}_e$ but decreases with I_p. While such variations, along with those in $\overline{\sigma v}_{iz}$ and the peaking factor, could be included in eqn.(10), in light of the fact that $\bar{v}_n$ is only estimated this is not warranted at this stage - and a constant (poloidally averaged) value of $\lambda_\Gamma = 30$ mm is assumed.

The result of inserting these estimated values into eqn.(10), namely $n_e(a) = 5\times10^{-21}\ \bar{n}_e^{\,2}$, is shown in fig. 7. As can be seen, the agreement is quite good both as to absolute magnitude and the gross trend of the data, which approximates to an $n_e(a) \propto \bar{n}_e^{\,2}$ relation. In fact experimental data, at constant edge temperature, show $n_e(a)$ to be proportional to $\bar{n}_e^{\,2}$ to within 10%. Detailed agreement between model and experiment is not found, however; in particular, there is a clear pattern of $n_e(a)$ rising less rapidly than $\bar{n}_e^{\,2}$, for a fixed I_p. At constant current ie, constant ohmic heating we have observed that the edge temperature falls as the density

rises, and thus it is unlikely that v_n is constant. Monte Carlo calculations of $\bar{v}_n$, in progress, are required to test the model in more detail. For the present, it is concluded that the mechanisms governing $n_e(a)$ appear to be described by a simple diffusion model.

The total particle flux to the limiter Γ_L, is given by the same modelling[17] as

$$\Gamma_L = \bar{n}_e^{\,2} A_p D_\perp \overline{\sigma v}_{iz} / 6 \bar{v}_n \qquad (11)$$

where A_p is the plasma surface area. Taking $D_\perp = 10^{19} / \bar{n}_e$ from fig.9 gives the line shown in fig.6, namely $\Gamma_L = 300\ \bar{n}_e$. Since the comparison of model and experiment is essentially the same one as made for $n_e(a)$, not surprisingly the agreement is also reasonable, both as to absolute magnitude and trend with $\bar{n}_e$. Again a full replication of the observed variation is not achieved.

Turning to the edge temperature $T_e(a)$, fig. 5, the simplest model is that

$$T_e(a) = -\frac{1}{e} \left(\frac{m_i}{2}\right)^{1/3} \left[\frac{P_L}{A\ \gamma\ n_e(a)}\right]^{2/3} \qquad (12)$$

where A is the area of the limiter interacting with the plasma. This equation is a modified form of equation (8) and as we have seen in section 3.1 it has been approximately confirmed experimentally.

Assuming $P_L \propto I_p$ and using equation (10) we obtain $T_e(a) \propto I_p^{\,2/3} / \bar{n}_e^{\,4/3}$, a relation which approximately reproduces the trend of fig.5, although less strong a variation than the observed $T_e(a) \propto (I_p / \bar{n}_e)^2$,

eqn.(3). A quantitative result is obtained by assuming that 50% of P_H is radiated, that $P_H = P_\Omega = I_p$, $V_{loop} \approx 0.7\ I_p$ and $\gamma_s = 10$ a constant, giving

$$T_e(a) = 1.1 \times 10^{23}\ I_p^{2/3} / \bar{n}_e^{4/3}\ \ [ev] \qquad (13)$$

This relation actually reproduces the magnitude of the experimental values of $T_e(a)$ to within about a factor of three, fig.5. We may conclude that the basic mechanisms governing the relation between the edge parameters and the global parameters on JET are roughly accounted for by a simple particle diffusion model plus energy conservation.

The effect of density on edge temperature in the absence of radiation, i.e. if impurity production were completely removed, can be deduced in a similar way. We simply assume that the power conducted to the edge is equal to the total input power. This leads to double the previous edge temperature but with the same parametric dependence as in equation 13.

The reasonable agreement between the model predictions for $n_e(a)$ and Γ_L, (eqns.(10), (11)) and observations would imply that particle balance is not very sensitive to the edge temperature. The apparent I_p-dependance of $n_e(a)$, Fig.7, is probably due to the operational coupling of $\bar{n}_e$ and I_p. On the other hand the energy balance quantities such as $T_e(a)$ are affected by the flow of particles into the edge, in fact $T_e(a) \propto \Gamma_L^{-1}$. In this sense one can say that the particle balance has a strong influence on energy balance, but not vice versa. This effect facilitates a more detailed examination of energy balance, as discussed in the next section.

4.3 More detailed modelling of energy balance

In the basic model the radiated power P_R was treated as a global parameter, ie part of the input rather than a predicted quantity. Since P_R

is due to impurities which are produced at the edge it is possible, in principle, to transfer this quantity from the category of input to a calculated quantity. This is undertaken in this section.

It is recognized that such a calculation is much more ambitious than the basic model and hence rather drastic simplifying assumptions have to be made. It is nevertheless valuable to see how a completely self-consistent model of the edge parameters can be derived in an analytical way and in particular to see what are the most important parameters determining edge conditions. It is hoped that this attempt may lead to a better understanding of the important factors determining impurity production rates.

Following the basic model we assume that the particle balance has a strong influence on energy balance, but not vice versa. It was also found that a detailed explanation of particle balance is not possible without a more detailed knowledge of neutral particle behaviour, eg $\overline{v}_n$. These two findings suggest that a suitable approach to a more detailed examination of energy balance would be to de-couple the two balances by treating the measured values of $n_e(a)$ and Γ_L as input to the model. The model would then seek to predict $T_e(a)$ and P_R with $\overline{n}_e$, Γ_L, I_p, etc. as input. This approach also avoids needing to know other quantities related to particle balance eg. the value of $D_\perp$.

The conducted power into the edge is given by eqn.(8). This equation can be rewritten as

$$T_e(a) = \frac{P_L}{e\gamma_s \Gamma_\parallel(a)\ H\ \lambda_p} \qquad (14)$$

In order to carry out the energy balance calculation we take from the basic

model that $n_e(a)$ is proportional to $\bar{n}_e^2$, which is consistent with the experimental data. $\Gamma_\parallel$ is then calculated using equation (1) resulting in a dependence of $\Gamma_\parallel$ on $\bar{n}_e$, somewhat stronger than observed experimentally, fig. 4. The effect of assuming a linear density relationship is discussed later.

The impurity sputtering rate is given by

$$R = \int_0^\infty H\ \Gamma_\parallel(r)\ Y(r)\ dr \tag{15}$$

where Y(r), the sputter yield, depends on $T_e(r)$. The ion energy is given by the sum of two terms, the thermal energy and the acceleration in the plasma sheath potential V_s. Assuming $T_e = T_i$

$$E \approx 2T_e + qV_s\ T_e \equiv KT_e \tag{16}$$

where q is the ion charge, $V_s = 0.5\ T_e\ \ln\left[\frac{2\pi m_e}{m_i}\frac{(1 + T_i/T_e)}{(1 - \delta)^2}\right]$ and δ is the secondary electron yield for primary electrons. For D^+, $T_e = T_i$, and $\delta = 0$ one obtains $K = 4.8$.

The sputtering yield can be obtained from a number of empirical formulae[19]. The simplest analytical form which gives a good fit to the data is[20]

$$Y(E) = \frac{Q(E - E_T)}{(E - E_T + B)^2} \tag{17}$$

where Q, E_T and B are fitting parameters which vary with the target

material and incident ion combination. Thus

$$R = \int_0^\infty \Gamma_\parallel(r) \frac{H\, Q(KT_e(r) - E_T)}{(KT_e(r) - E_T + B)^2} dr. \qquad (18)$$

We now have the sputtering rate in terms of the power conducted to the edge using eqn.(14). If we consider the sputter rate as the major impurity source then this impurity generation rate can be related to the impurity concentration in the plasma and hence to the power radiated.

We consider a simple global model for the impurity concentration similar to that used for the plasma ions in section 4.2. Using the Engelhardt diffusion model[16] we obtain for the impurity density throughout most of the plasma

$$n_m = \frac{R(\lambda_i^m + \lambda_\Gamma)}{A_p\, D_\perp} \qquad (19)$$

where λ_i^m is the ionisation mean free path for impurities, and λ_Γ is the e-folding length for the impurity flux in the SOL. The λ_Γ term represents the strength of the SOL sink for impurities flowing to the limiter and is assumed here to be the same as for the deuterium ions. It is assumed that there is no inward pinch, i.e. the impurity density profile is flat.

The power radiated by the impurities is given by

$$P_R = \int_0^a n_m(r)\, n_e(r)\, 4\pi^2 Rr\, L(T)\, dr \qquad (20)$$

$$\approx \bar{n}_m\, \bar{n}_e\, V_p\, \bar{L}(T) \qquad (21)$$

where $\bar{n}_m$ and $\bar{n}_e$ are average values of the impurity and electron density and $\bar{L}(T)$ is a mean radiation constant averaged over the plasma of volume V_p. In JET and ASDEX the radiated power has been found to be given approximately by an expression of the form[21]

$$P_R = 10^{-35} A_p \bar{n}_e^{\,2} (Z_{eff}-1) \quad W\ m^4$$

For carbon impurity this can easily be shown to correspond to a volume averaged radiation constant $\bar{L}(T) = 0.4 \times 10^{-33}$ W m^3. Substituting for n_m from equation (19) into equation (21) we obtain

$$P_R = \bar{n}_e \frac{V_p}{A_p} \frac{\bar{L}(T)}{D_\perp} (\lambda_i^m + \lambda_\Gamma)\, R \qquad (22)$$

Using equations (14) and (18) for R we now have the expression for P_R in terms of P_L. Rewriting eq.(8) and allowing for $P_H \geq P_\Omega$

$$P_L + \frac{V_p(\lambda_i^m + \lambda_\Gamma)}{A_p D_\perp} R.\bar{n}_e.\bar{L}(T) = P_H \qquad (23)$$

Since by combining eqns.(14) and (18) R can be expressed in terms of P_L, equation (23) can be solved numerically to obtain P_L and P_R for a given input power, and hence to obtain T_e. λ_i^m remains approximately constant for the range of conditions used experimentally because the increasing density and the decreasing temperature (and hence ionisation rate coefficient) just balance[22]. Typical values of λ_i^m are 0.02 m. λ_Γ the e-folding length for impurities is assumed to be the same as for plasma ions i.e. $\approx$ 0.03 m poloidally averaged. We also assume that all ions arrive with an energy

determined by the leading edge temperature and equation 16. Sputtering due to fuel ions (D or He) as well as self-sputtering are included. For self-sputtering the carbon ions are taken to be 4 times ionised, though results are not very sensitive to the charge state. The radiation constant $\bar{L}(T)$ has been varied from 0.2×10^{-33} to 1×10^{-33}. The results, figs. 10 and 11, are shown for $\bar{L}(T) = 0.5\times10^{-33}$ W m^3.

From the results in fig.10 we see that as the power increases for a given density the edge temperature increases and as the density increases the edge temperature decreases, in the same quantitative way as the basic model (eqn.13) and the experimental results. The temperature dependence is on average $T_e(a) \propto \bar{n}_e^{-1.7}$ which is stronger than the $\bar{n}_e^{-1.33}$ dependence deduced for the simpler model, section 4.2. This increase in negative slope reflects the effect of sputtering and radiation. The effect is relatively small for the case of carbon impurities discussed here, but is more important for higher z materials. The effect of choosing a linear relationship between $n_e(a)$ and $\bar{n}_e$ has been discussed previously[12]. It results in a similar set of curves, but a less rapid change of $T_e(a)$ with density.

At low density there is probably an upper limit to the edge temperature determined by the onset of arcing or possibly increased secondary electron emission leading to high power density on the limiters. Since little power is radiated all the power goes to the limiters and there may be melting or sublimation. An upper limit to the edge temperature clearly sets a lower density limit for a given power level. The results of fig.10 are similar
to those given by eqn.(13) - but now, of course, P_R is calculated rather than assumed as input.

The scaling of the radiated power with density is another interesting prediction of the model, fig.11. At low densities the edge temperature is high and the sputter yield is at its maximum, plateau, value and is thus almost independent of density. The influx of impurities and hence the impurity concentration is thus constant and the power radiated increases linearly with the electron density. Since the sputter yield has reached its maximum value, increasing the input power does not increase the impurity concentration and the radiated power is almost independent of the input power. Thus the power radiated as a fraction of the input power decreases as the input power increases. At high densities the edge temperature and hence the impurity influx falls with increasing density so that the impurity concentration falls and the radiation as a function of the input power reaches an approximately constant value. This is in agreement with both JET data and data from other tokamak experiments[23, 24, 25]. The radiation plateau in JET does not cover a very wide density range (fig.10) but the fact that the plateau comes at the correct density and is ~ 50% of the total radiation level is encouraging.

When the density increases further the edge temperature decreases to a value at which the ion energy almost reaches the threshold for sputtering. The impurity density drops more rapidly than the density rises and the total radiation is predicted to fall, fig.11. This is not observed experimentally. What happens is that the temperature profile collapses[26] and leads to an mhd instability as described by Wesson et al[27]. The assumption of a constant value if L(T) becomes invalid and the power radiated actually increases to 100%. These effects are not included in the present model. However it is interesting to note in fig.11 how the density at which the edge temperature drops to a given value increases with increasing power. If we assume that there is a critical temperature at

which the radiation collapse takes place then fig.11 gives a qualitative picture of how the density limit increases with increasing input power.

4.4 Comparison with helium discharges

A small amount of data is available for discharges in both ^3He and ^4He. In some cases, particularly at low plasma currents the edge temperatures are higher than in deuterium discharges. This rather surprising result is not predicted by the model. Because of the higher sputter yield for helium for the same ion flux the number of sputtered impurity atoms would be expected to be higher. This causes the radiation to be large and hence to reduce the energy convected to the boundary layer. The model predicts that the power radiated should be significantly higher in helium discharges than in deuterium.

From spectroscopic measurements it is clear that the oxygen concentration is much lower in helium than in deuterium discharges[28]. This would explain the higher edge temperatures. A possible candidate for the oxygen production mechanism is charge exchange neutral fluxes leading to gas desorption from the walls e.g. CO, CO_2 and H_2O. Experimental measurements have shown the total CX fluxes to be 5 to 15 x higher in deuterium than in helium discharges[29]. The relative desorption cross section for deuterium and helium atoms is however not known.

Conclusion

Measurements of the edge densities and temperatures in JET show that there is a clear scaling of these parameters with average plasma density and with input power. Simple analytical models give reasonable agreement with the experimental measurements without use of any arbitrary constants. Over the wide range of powers used the broad trend is for the edge density $n_e(a)$ to increase as the square of the average density, but for a given

power input the edge density increases more slowly, approximately linearly with the average density. This may be due to the change in the edge temperature leading to a change in the velocity of the recycling neutrals.

The experimentally measured edge temperature decreases approximately as $\bar{n}_e^{-2}$ while the simple models described give an approximately $\bar{n}_e^{-1.3}$ dependence. When the effect of sputtering is included the density dependence becomes stronger $\sim \bar{n}_e^{-1.7}$, in better agreement with experiment. The models predict that the edge temperature should increase with increasing input power roughly as P_H. Experimentally with ohmic heating the edge temperature increases more rapidly, typically as P_H^2. This may be due to the experimentally observed decrease in the SOL thickness as the plasma current is increased[30], which is not included in the modelling. The effect is at least partly due to the change in the connection length in the SOL due to a change in the safety factor q. The decrease in the SOL thickness decreases the effective limiter interaction area and thus increases the edge temperature required to transfer a given heating power. Such an effect is not expected for additional heating power (eg NBI or ICRH). Thus the modelling has been carried out in terms of power scaling even though for the ohmic data presented here the more obvious experimental parameter is the current. Preliminary data for the scaling of edge temperature with neutral beam heating give results in reasonable agreement with the simple model[30].

As density is decreased the edge temperature rises. However, for the range of input powers there appears to be an upper limit to the edge temperature observed ~ 200 eV. This may be a real physical limit due either to the onset of arcing or to high secondary electron emission leading to a high sheath power transmission factor. An upper limit to the edge temperature combined with the scaling we have observed leads to a

lower density limit which depends on the input power ie as input power increases so does the minimum density obtainable.

While the modelling is clearly over-simplified, neglecting the contribution of other impurities such as oxygen to the radiation and of any changes in the impurity radial profiles, it gives a generally satisfactory description of the main features of the edge parameters. The scaling laws should be generally useful in extrapolating to both higher densities and powers. Further analysis of data in helium discharges and with additional heating is important to determine the range of applicability of the scaling.

References

1. ERENTS, S.K., TAGLE, J.A., McCRACKEN, G.M., STANGEBY, P.C., DE KOCK, L., Nuclear Fusion 26 (1986) 1591.
2. ALEXANDER, K.F., GUNTHER, K., HINTZE, W., LAUX, M., PECH, P., REINER, H-D., CHANKIN, A.V., Nuclear Fusion 26 (1986) 1575.
3. BUDNY, R.V., HEIFETZ, D.B., KILPATRICK, S., MANOS, D., OWENS., D.K., PAPES, R., STANGEBY, P.C. ULRICKSON, M., J. Nucl. Mat. 145-147 (1987) 245.
4. McCRACKEN, G.M., STANGEBY, P.C., Plasma Physics and Controlled Fusion 27 (1985) 1411.
5. BRINKSCHULTE, TAGLE, J.A., BURES, M., ERENTS, S.K. et al. 13th European Conf. on Controlled Fusion and Plasma Heating, Schliersee (1986) Vol. 1, 403.
6. TAGLE, J.A., Course on Basic and advanced diagnostics Summer School Varenna 1986 to be published.
7. TAGLE, J.A., ERENTS, S.K., McCRACKEN, G.M., PITTS, R.A., STANGEBY, P.C., LOWRY, C., STAMP, H.F., 14th European Conference on Controlled Fusion and Plasma Physics, Madrid 1987, Vol.II 1987 662.
8. MATTHEWS, G.F., McCRACKEN, G.M., SEWELL, P., WOODS, M., HOPKINS, B.J., J. Nucl. Mat. 145 and 146 (1987) 225.
9. WOODS, M.E., HOPKINS, B.J., MATTHEWS, G.F., McCRACKEN, G.M., SEWELL, P., FAHRANG, H., J. Phys. D. 1987 to be published.
10. SUMMERS, D.R., private communication.
11. MAST, K.F., KRAUSE, H., BEHRINGER, K., BULLIARD, A., MAGYAR, G., Rev. Sci. Instrum. 56 (1985) 969.
12. RUZIC, D.N., HEIFITZ, D.B., COHEN, S.A.,J. Nucl. Mat. 145 and 146 (1987) 527.

13. STANGEBY, P.C., TAGLE, J.A., ERENTS, S.K., LOWRY, C., 14th European Conference on Controlled Fusion and Plasma Physics, Madrid 1987, Vol.II (1987) 670.

14. McCRACKEN, G.M., FIELDING, S.J., OHTSUKA, H., J. Nucl. Mat. 111 and 112 (1982) 396.

15. NEUHAUSER, J., LACKNER, K., WUNDERLICH, R., IPP Report 1/198 (1982), Max Planck Institut, Garching.

16. ENGELHARDT, W., et al, J. Nucl. Mat. 111 and 112 (1982), 337.

17. STANGEBY, P.C., J. Nucl. Mat. 145 and 146 (1987), 105.

18. HEIFETZ, D.B., et al, J. Comp. Phys. 46 (1982), 309.

19. ROTH, J., in Physics of Plasma Wall in Controlled fusion Ed. D.E. Post and R. Behrisch NATO ASI Series Plenum Press New York 1984. pg 351.

20. SMITH, D.L., BROOKS, J.N., POST, D.E., HEIFETZ, D., Proc. 9th Symp on Eng. Problems of Fusion Research Chicago 1981, IEEE NY (1982), 719.

21. BEHRINGER, K., BOILEAU, A., BOMBARDA, F., et al, Plasma Physics and Controlled Nuclear Fusion, (Proc. 11th Int. Conf. Kyoto 1986) paper IAEA CN47/A.

22. McCRACKEN, G.M., Plasma Physics and Controlled Fusion (Proc. EPS Madrid Conference, June 1987). To be published.

23. BICKERTON, R.J., ALLADIO, F., BARTLETT, D.V., et al. Plasma Physics and Controlled Fusion, 28, (1986) 55.

24. MATTHEWS, G.F., McCRACKEN, G.M., GOODALL, D.H.J., PITCHER, C.S., et al., Plasma Physics and Controlled Fusion (Proc. EPS Madrid Conference, June 1987). To be published.

25. JOYCE, B., LISTER, J.B., MARET, J.M., NOWAK, S., Plasma Physics and Controlled Fusion 29, (1987), 27.

26. GIBSON, A., Nuclear Fusion 16 (1976) 546.

27. WESSON, J.A., GOWERS, C., HAN, W., MAST, F., et al. Controlled Fusion and Plasma Physics (13th European Conference Budapest 1986) Vol.1 p.147.

28. BEHRINGER, K.H., Impurity Topic Report 1987. Unpublished.

29. VERBEEK, H., et al, J. Nucl. Mat. 145 and 146 (1987), 523.

30. ERENTS, S.K., TAGLE, J.A., McCRACKEN, G.M., Plasma Physics and Controlled Fusion (Proc. EPS Madrid Conference, June 1987). To be published.

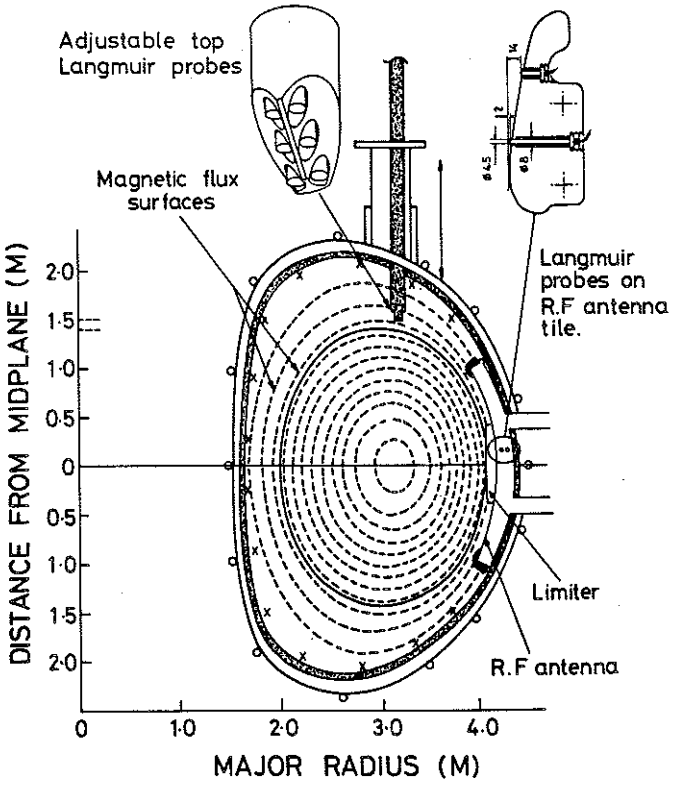

Fig. 1 Cross section of the JET vacuum vessel showing limiter, RF antenna and the two sets of Langmuir probes. The magnetic flux surfaces are shown calculated for a discharge with plasma current $I_p = 3.1\,\mathrm{MA}$.

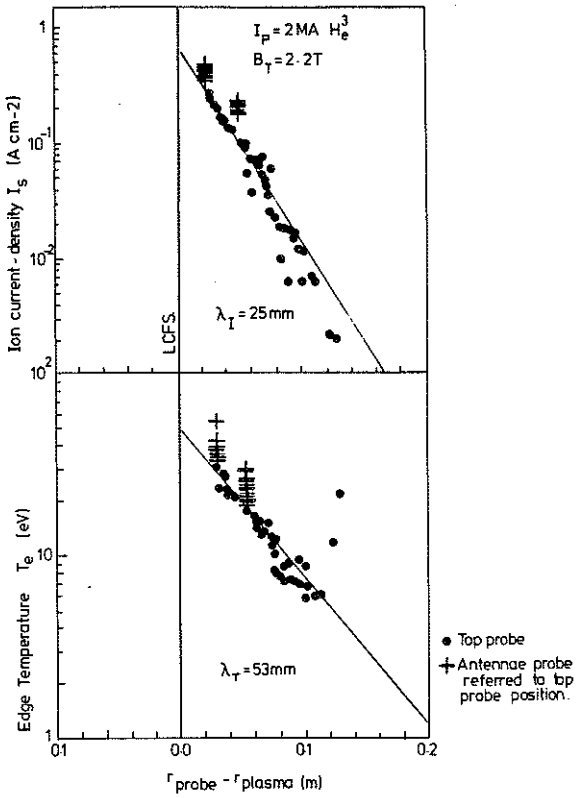

Fig. 2 Radial profile of the ion saturation current I_s and the electron temperature T_e in the SOL, as measured with top probes and the antenna probes. $I_p = 2\,\mathrm{MA}$, $B_T = 2.2\,\mathrm{T}$, $\bar{n}_e = 1.8 \times 10^{19}\,\mathrm{m}^{-3}$.

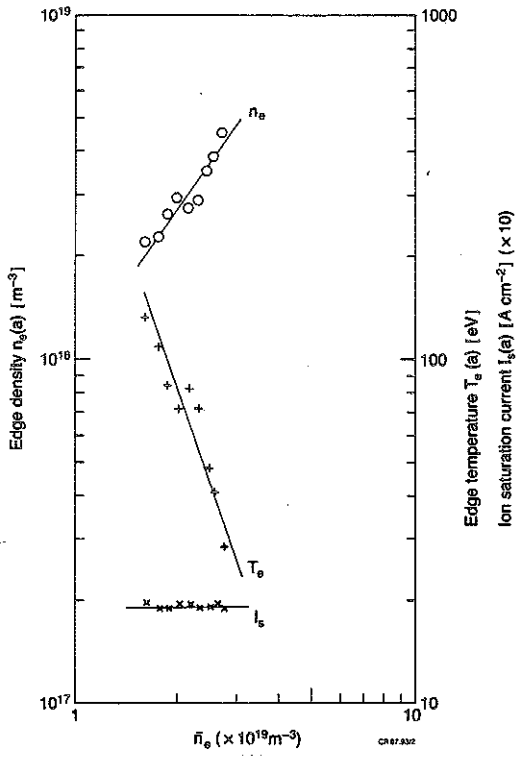

Fig. 3 Variation with line average plasma density of ion saturation current, electron temperature and calculated $\bar{n}_e$, extrapolated to the last closed flux surface. $I_p = 3$MA, $B_T = 2.9$T.

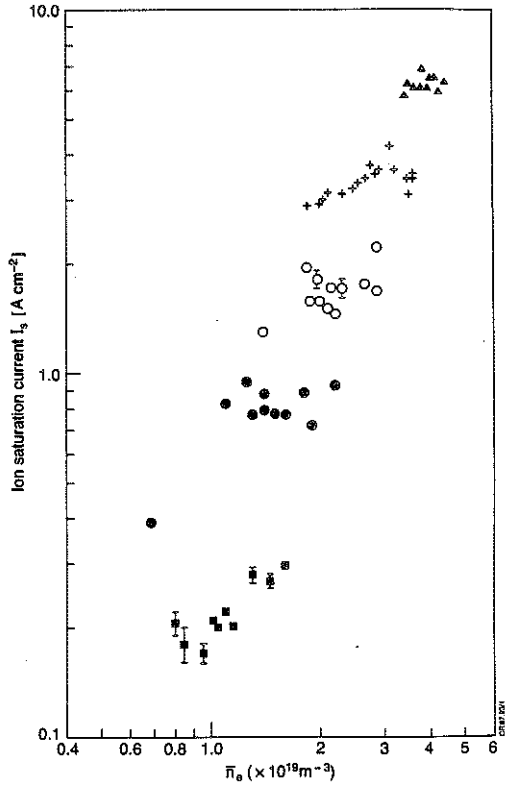

Fig. 4 Ion saturation current at the LCFS as a function of line average density for a range of plasma currents. ▪ 1MA, ● 2MA, ○ 3MA, + 4MA, Δ 5MA.

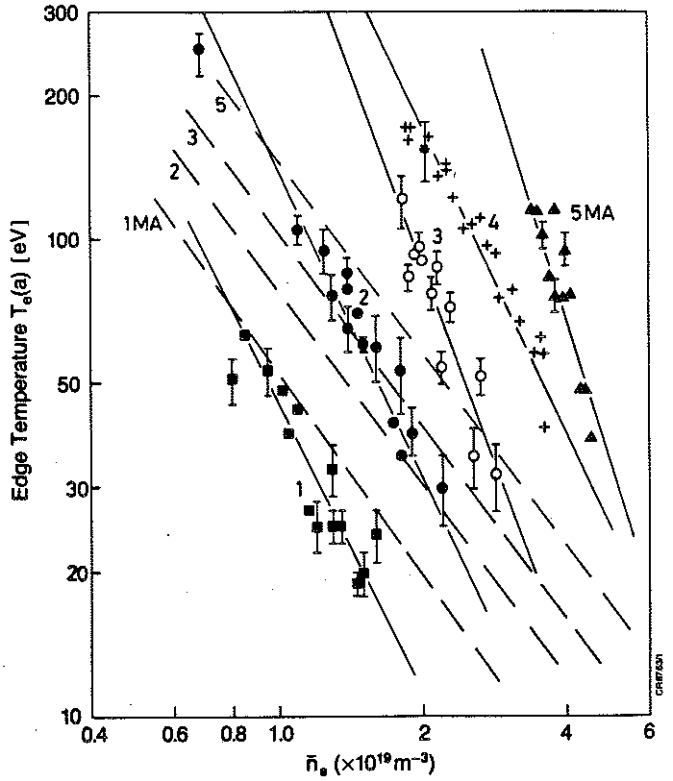

Fig. 5 Electron temperature at the LCFS as a fraction of line average density for a range of plasma currents.
▪ 1MA, ● 2MA, ○ 3MA, + 4MA, Δ 5MA.
---Predictions from equation 13.

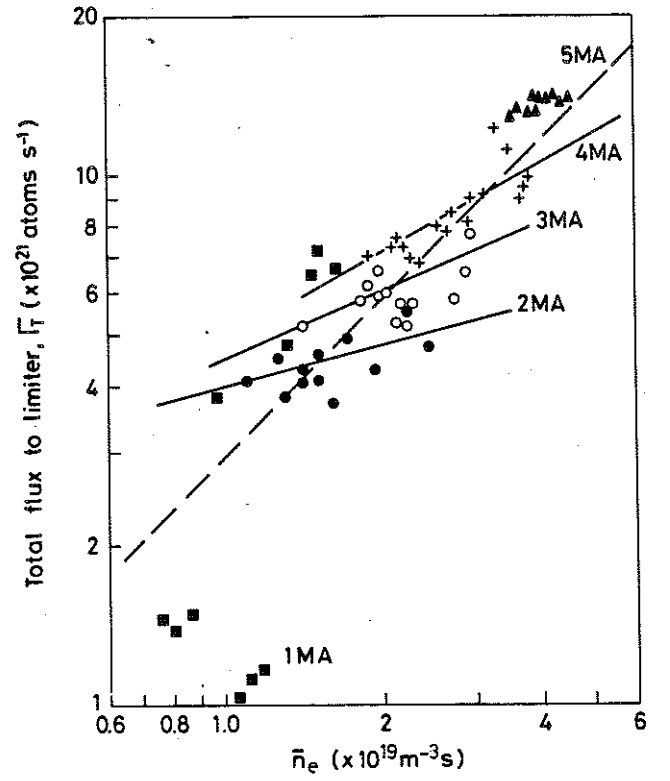

Fig. 6 Total flux of ions arriving at the limiter calculated from the radial profiles of I_s using equation (4) and experimental data.
---Predictions from equation 11.

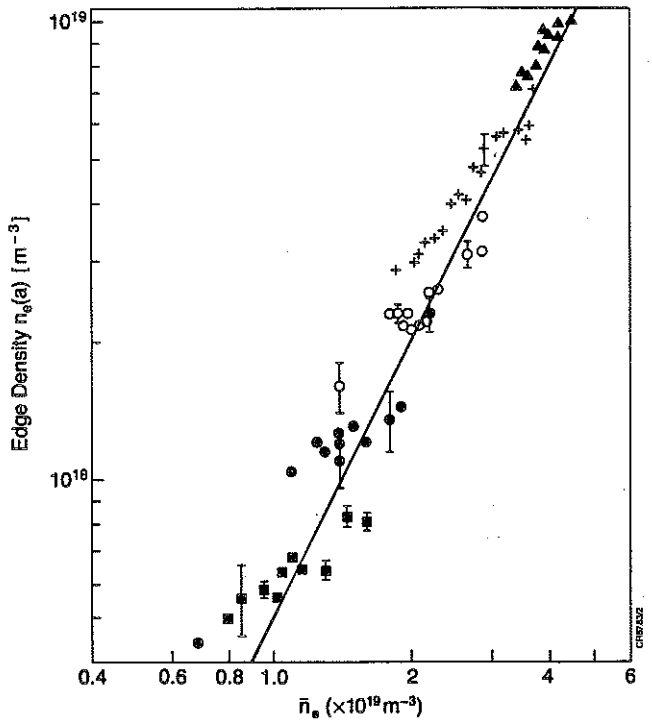

Fig. 7 Edge density at the LCFS, calculated from I_s and T_e assuming $T_e = T_i$, as a fraction of line average density for various plasma currents.
▪ 1MA, ● 2MA, ○ 3MA, + 4MA, Δ 5MA.
— Predictions from equation 10.

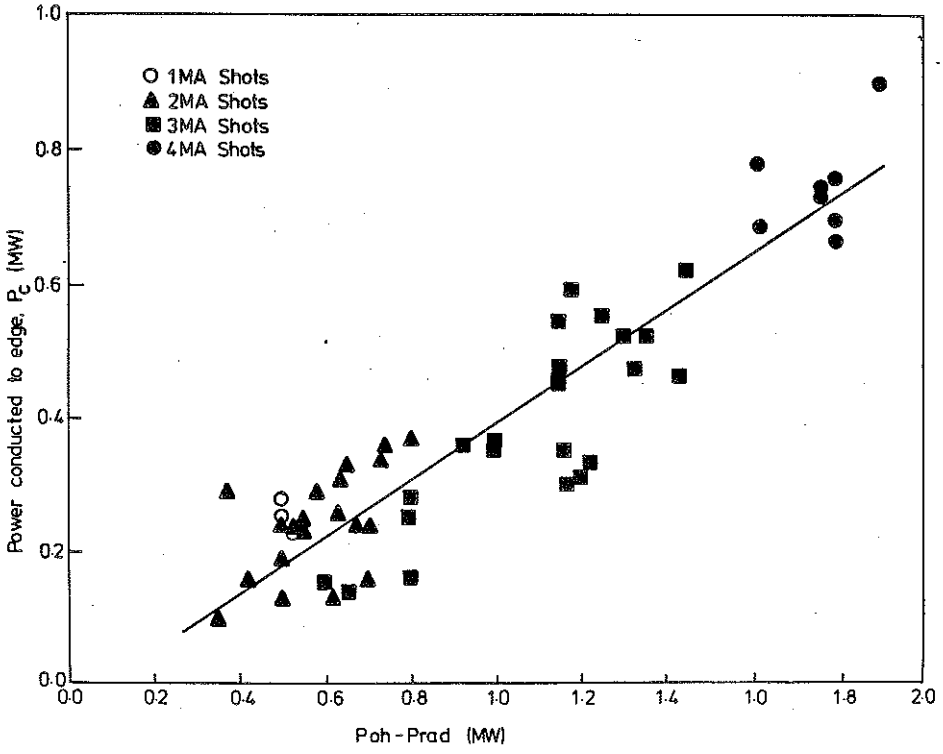

Fig. 8 Power conducted to the edge, calculated from experimental measurements of I_s and T_e, integrated over radial and toroidal directions as a function of (power input—power radiated) for a range of plasma currents.

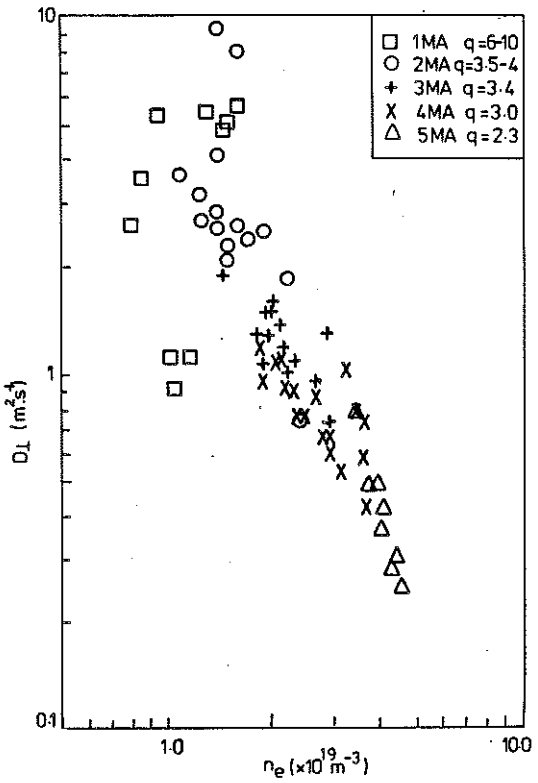

Fig. 9 Cross field diffusion rate $D_\perp$ calculated from the density e-folding length according to equation 9.

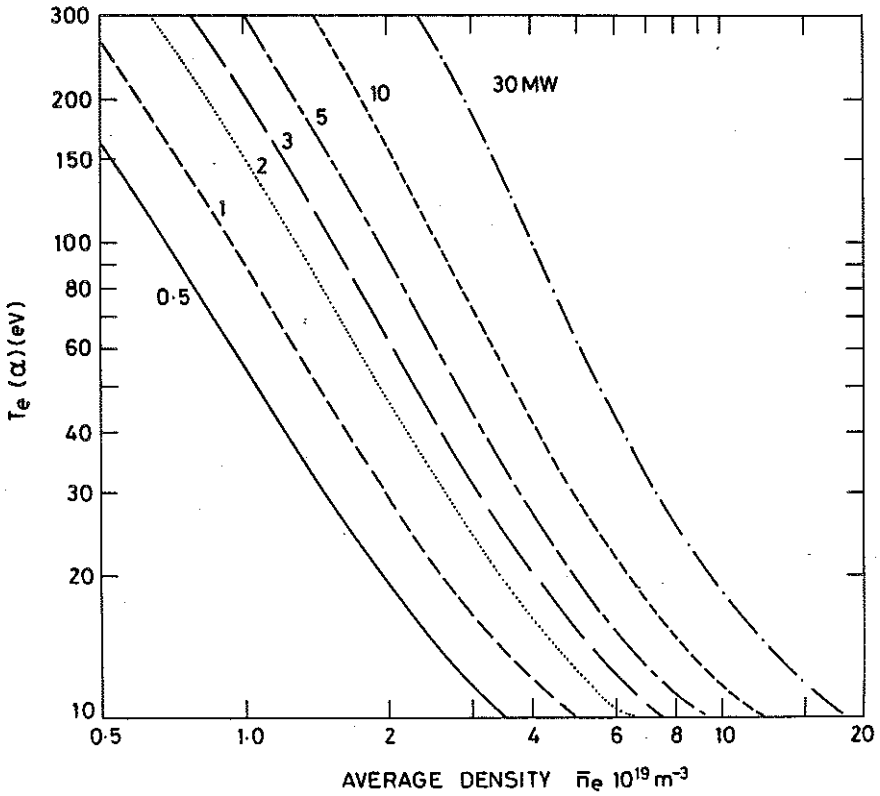

Fig. 10 Calculation of the edge temperature in JET based on limiter sputtering and self sputtering of carbon assuming an average radiation constant of $L(T)=0.5\times10^{-33}$ w m^{+3} for various input powers.

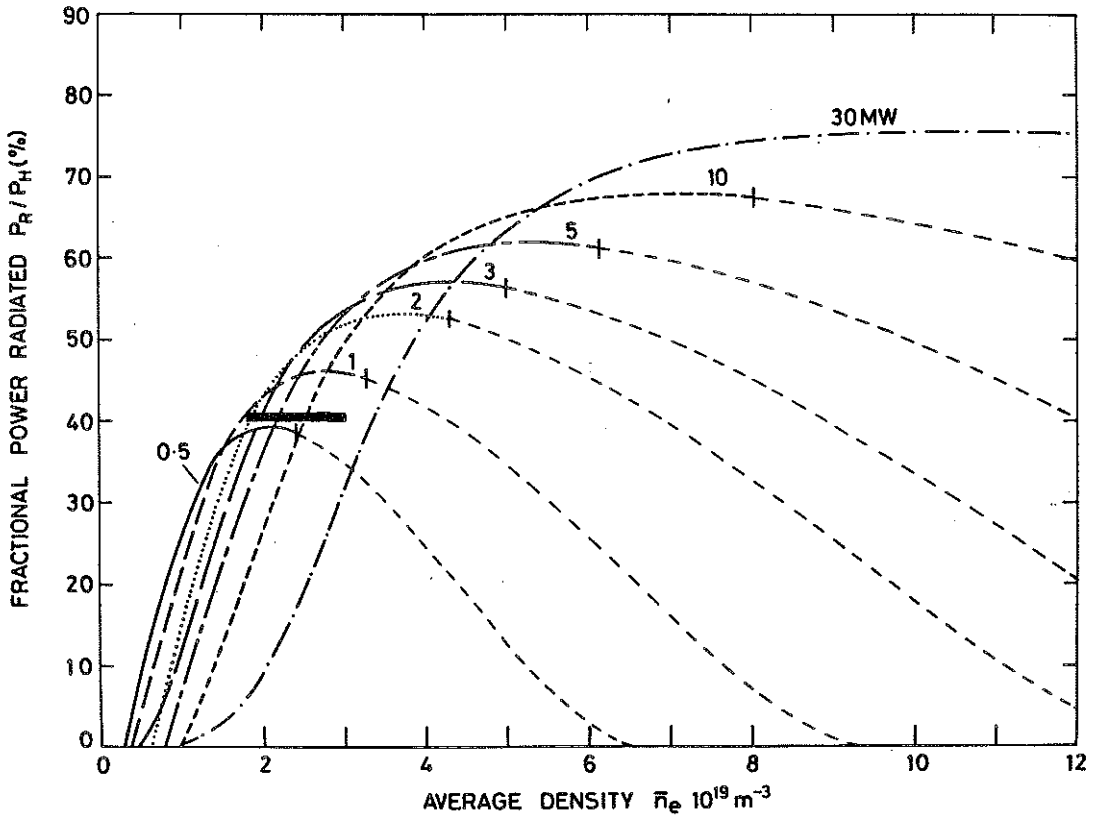

Fig. 11 Calculation of the fractional power radiated in JET using the limiter sputtering model assuming an average radiation constant $L(T)=0.5\times10^{-33}$ wm^3 for various input powers. JET experimental data at ~3MA. Dashed lines ---- indicate the density range over which the edge temperature is less than 15eV.